JOURNAL OF GEOPHYSICAL RESEARCH, VOL. 115, D00H17, doi:10.1029/2009JD012046, 2010

Relationships among properties of marine stratocumulus derived from collocated CALIPSO and MODIS observations

C. R. Hayes,[1] J. A. Coakley Jr.,[1] and W. R. Tahnk[1]

Received 12 March 2009; revised 18 September 2009; accepted 23 October 2009; published 27 March 2010.

[1] Collocated Moderate Resolution Imaging Spectroradiometer (MODIS) imagery and Cloud-Aerosol Lidar and Infrared Pathfinder Satellite Observation (CALIPSO) 532 nm total attenuated backscatter coefficients were used to identify 50 km scale segments for ocean regions that had only a single layer of marine stratocumulus. On the basis of whether the underlying ocean surface was detected in the backscatter coefficients, the segments were separated into those for which all of the 1 km MODIS pixels were identified as being overcast (no surface detected) and those for which there were breaks in the cloud layer (surface detected). Cloud properties for the collocated MODIS pixels were obtained from the MODIS MOD06 cloud product and from a retrieval scheme designed to account for broken clouds within imager pixels. For the 50 km overcast segments the variations in optical depth, τ, and droplet effective radius, R_e, obtained from the MOD06 and partly cloudy pixel retrievals were in agreement, and the variations in layer temperature were consistent with those inferred from the CALIPSO backscatter coefficients. In addition, the droplet effective radii retrieved separately using the 1.6, 2.1, and 3.7 μm MODIS reflectances were consistent with droplets growing as clouds thickened and mean values of $d\ln R_e/d\ln\tau$ were close to 0.2, as predicted by adiabatic cloud parcel models. When the segments contained broken clouds, however, the droplet effective radii for the three near-infrared wavelengths were inconsistent with droplets growing as clouds thickened and $d\ln R_e/d\ln\tau$ departed from 0.2. This breakdown is thought to result from biases in the retrieved cloud properties caused by subpixel-scale variations in liquid water amount and droplet radius.

Citation: Hayes, C. R., J. A. Coakley Jr., and W. R. Tahnk (2010), Relationships among properties of marine stratocumulus derived from collocated CALIPSO and MODIS observations, *J. Geophys. Res.*, *115*, D00H17, doi:10.1029/2009JD012046.

1. Introduction

[2] Marine stratus and stratocumulus reflect a sizable fraction of the incident sunlight while having little effect on the thermal radiation that the Earth emits. Such clouds are plentiful and exert a strong influence on Earth's radiation budget and consequently on climate and climate change [*Hartmann et al.*, 1992; *Bony and Dufresne*, 2005]. While perhaps the simplest of cloud systems to model, the need to account for processes on small time and space scales to capture the behavior of marine stratocumulus makes the task of developing parametric schemes for climate models seemingly futile [*Randall et al.*, 2003]. Nonetheless, the wealth of cloud properties derived from satellites during the past decade holds the promise of providing critical assessments of model generated clouds.

[3] Unfortunately, the same small time and space scale processes that make parametric schemes for marine stratocumulus difficult to develop also make the retrievals of their cloud properties prone to error. Small-scale variability within imager pixels [*Cahalan et al.*, 1994; *Loeb and Coakley*, 1998], not to mention fractional cloud cover within the pixels [*Han et al.*, 1994; *Platnick et al.*, 2003; *Coakley et al.*, 2005; *Kato et al.*, 2006], give rise to biases in the retrieved properties that hamper assessments of model performance. For example, in the case of marine stratus and stratocumulus, adiabatic cloud parcel models have gained popularity in predicting relationships between droplet radius, visible optical depth, and cloud thickness [*Brenguier et al.*, 2000; *Szczodrak et al.*, 2001]. *Boers et al.* [2006] generalized these models so that effects due to mixing could be included. In such models, the droplet number concentration at the lifting condensation level is held constant. Water vapor condenses on the nuclei as the air ascends from the base of the cloud. In adiabatic ascent the liquid water content increases linearly with height above the lifting condensation level. Since the number concentration is held constant, droplet volume becomes proportional to cloud thickness and optical depth becomes linked to droplet radius. The relationships that arise among the cloud properties have been used to derive cloud thickness and number concentrations on the basis of retrieved

[1]College of Oceanic and Atmospheric Sciences, Oregon State University, Corvallis, Oregon, USA.

0148-0227/10/2009JD012046

droplet effective radius and visible optical depths. Some have noted, however, that the expected relationships are not observed when the fields of view of the sensors are too coarse to account for broken clouds [*Szczodrak et al.*, 2001; *Harshvardhan et al.*, 2004; *Schüller et al.*, 2005].

[4] Here assessments are made of the cloud properties obtained from the Moderate Resolution Imaging Spectroradiometer (MODIS) MOD06 cloud product and a partly cloudy pixel retrieval scheme [*Coakley et al.*, 2005] in conjunction with the Cloud-Aerosol Lidar and Infrared Pathfinder Satellite Observation (CALIPSO) lidar. The MOD06 cloud properties are derived assuming that the 1 km nadir resolution MODIS pixels are overcast when clouds are detected. As was mentioned earlier, for partly cloudy pixels this assumption is known to lead to biases in the retrieved cloud properties. The partly cloudy pixel retrieval scheme was developed to account for effects caused by the partial covering of a pixel by clouds. The retrievals are strictly applicable to single-layered cloud systems such as marine stratocumulus. The assumption is that clouds which only partly cover pixels are at the same altitude as the clouds that completely cover nearby pixels. The altitude of the layer is inferred from those of the overcast pixels within the region containing the partly cloudy pixels. The radiances in the partly cloudy pixels are then scaled linearly with fractional cloud cover to determine the radiances associated with the cloudy portions of the pixels. The radiances associated with the cloudy portions are then used to derive the cloud properties. The 532 nm total attenuated backscatter coefficients obtained with the CALIPSO lidar are collocated with Aqua MODIS pixels and used to identify MODIS pixels as either "overcast" by a single-layered system of marine stratus or only "partly cloudy," containing stratocumulus from a broken stratus layer. Pixels are identified as "overcast" if the lidar beam is attenuated so that the underlying ocean surface is undetected. Pixels are identified as "partly cloudy" if the lidar beam penetrates the cloud and the underlying ocean surface is detected. These distinctions are clearly arbitrary. The sampling by the CALIPSO lidar, a 70 m footprint spaced every 1/3 km, can miss holes in otherwise optically thick clouds. Likewise, penetrations that allow surface returns to be detected in the presence of clouds may simply indicate that the cloud is thin where the lidar beam penetrates, not broken. Nonetheless, as the results will suggest, the probability that a MODIS pixel identified as being "overcast" by marine stratus stands a high probability of being overcast. Likewise, a pixel found to be "partly cloudy" in an ocean region containing only a single layer of low-level clouds stands a high probability of being partly cloudy.

[5] The partly cloudy pixel retrieval scheme was applied to the Aqua MODIS level 1B calibrated radiances to identify 50 km scale regions that contained only a single layer of marine stratus or stratocumulus. Threshold schemes were developed and then applied to the CALIPSO 532 nm total attenuated backscatter coefficients to verify that the selected regions contained no other clouds but the layer of stratus or stratocumulus and then to identify the MODIS pixels that were either overcast, partly cloud covered, or cloud free. Optical depths, droplet effective radii, and cloud layer temperatures were obtained from the MOD06 cloud product and the partly cloudy pixel retrievals. In the case of the partly cloudy pixel retrievals, the pixel-scale fractional cloud cover was compared with the CALIPSO lidar identification of the partly cloudy and overcast pixels. On the assumption that across a 50 km scale region the large-scale thermodynamic environment was on average the same for all clouds within the region, departures of the cloud properties from their mean values for the overcast pixels were analyzed separately for the pixels found to be overcast and those found to be partly cloudy. This separation then allowed an assessment of whether the relationships among droplet radius, optical depth, and cloud thickness as predicted by adiabatic cloud parcel models fail to appear when the pixels become partly cloudy as suggested by earlier studies [*Szczodrak et al.*, 2001; *Harshvardhanet al.*, 2004; *Schüller et al.*, 2005].

2. Data Analysis

[6] The MODIS Aqua and CALIPSO observations were collected for 127 days between 13 June and 31 October 2006. The CALIPSO observations came from 373 daytime orbital passes. Because the optical depths, droplet radii, and layer altitudes of marine stratocumulus retrieved from MODIS radiances require observations of reflected sunlight, the collocated CALIPSO observations were restricted to daytime passes. The observations were over oceans off western continental margins, predominantly the west coasts of Africa and Europe (30°E–40°W, 60°S–60°N) and North and South America (70°W–150°W, 60°S–60°). These regions are frequented by marine stratus and stratocumulus [*Klein and Hartmann*, 1993]. Level 1B and level 2 (MOD06) MODIS collection 5 data were obtained from the NASA Goddard Space Flight Center level 1 atmosphere and archive distribution system. The partly cloudy pixel retrieval scheme was applied to the MODIS level 1B calibrated radiances. Following the approach described by *Matheson et al.* [2005], MODIS level 1B radiances and the retrieved cloud properties were analyzed to identify 50 km scale regions that contained low-level, single-layered clouds.

[7] CALIPSO level 1 and 2 data were analyzed in conjunction with the MODIS observations. CALIPSO level 1B data consist of reconstructed geolocated instrument data processed to sensor units at full resolution [*Winker et al.*, 2010]. Included in the level 1B data are profiles of total attenuated backscatter coefficients at 532 and 1064 nm, and perpendicularly polarized attenuated backscatter coefficients at 532 nm. Level 1B data are time referenced and include ancillary information consisting of radiometric and geometric calibration coefficients and analyzed profiles of temperature, pressure, and density. The level 2 lidar cloud and aerosol layer product data include derived geophysical variables such as column and layer properties. As CALIPSO level 2 cloud altitude data were not initially available for this study, a threshold-based cloud detection scheme was used to determine cloud top altitudes from the 532 nm total attenuated backscatter coefficients. When it became available, information on cloud altitude was obtained from CALIPSO level 2 data and compared with the altitudes derived from the cloud top detection scheme.

2.1. Collocation of CALIPSO and MODIS Observations

[8] The first step in collocating CALIPSO and MODIS observations was to identify candidate regions. A combina-

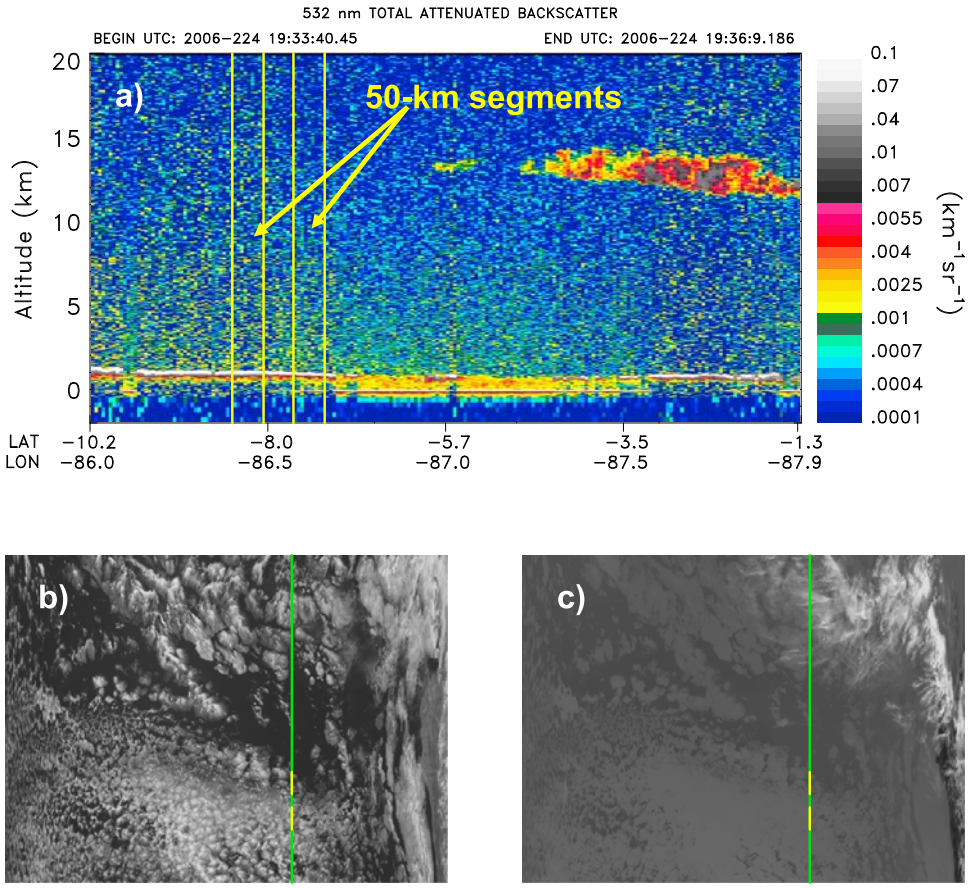

Figure 1. (a) The 532 nm total attenuated backscatter coefficient obtained from the CALIPSO lidar, (b) image of 1 km, 0.84 μm reflectances, and (c) emitted 11 μm radiances from Aqua MODIS for an overpass off the coast of South America at 1935 UT on 12 August 2006. The pass covers approximately 1000 km. Indicated in the backscatter coefficients are 50 km scale segments containing no other clouds but a single layer of low-level marine stratocumulus. In one of the segments the clouds completely cover the pixels, and in the other, there are breaks in the clouds as indicated by the presence of surface lidar returns in the CALIPSO data. The track of CALIPSO lidar observations is indicated in the images along with the two 50 km segments indicated in the backscatter coefficients.

tion of scene identification and layer tests described in the work of *Coakley et al.* [2005] and *Matheson et al.* [2005] were used to identify low-level, single-layered cloud systems over oceans. The modifications to the partly cloudy pixel retrieval scheme for its application to MODIS radiances used in this study were described in the work of *Segrin et al.* [2007]. Image granules were divided into 50 × 50 arrays of the MODIS 1 km pixels. The arrays selected for analysis were required to have no more than 10% land and valid partly cloudy pixel retrievals for at least 80% of the pixels. The valid retrievals included those for cloud-free pixels, pixels overcast by clouds in a single layer, and partly cloudy pixels which were assumed to be part of the same layer as the clouds in nearby overcast pixels.

[9] Of the 50 km scale regions that contained single-layered marine stratus and stratocumulus, the collocation of MODIS pixels and CALIPSO lidar beam was examined only for regions having a central latitude and longitude within 40 km of the track laid by the CALIPSO lidar beam on the ocean surface. Within these regions an automated routine was used to match the latitudes and longitudes associated with the lidar beam to those associated with the MODIS pixels.

[10] Figure 1 shows an example of a 1000 km collocated CALIPSO and MODIS scene. The scene is located off the west coast of Peru on 12 August 2006. Green lines in the MODIS images mark the path of the CALIPSO lidar with the two 50 km regions indicated in yellow. The cirrus cloud between 10 and 15 km in the CALIPSO scene clearly affects the 11 μm infrared wavelength but is difficult to detect in reflected sunlight at 0.84 μm. CALIPSO's sensitivity to these upper level clouds was used to identify multilayered cloud systems that may not have been detected by the single-layer tests applied to the MODIS data. Cirrus and midlevel cloud filters were developed and used with the CALIPSO observations for each 50 km region.

2.2. Upper and Middle-Level Cloud Filters Applied to CALIPSO Lidar Returns

[11] A scheme was developed to detect thin upper level clouds, primarily cirrus, above 8.2 km and midlevel clouds between 5 and 8.2 km using the CALIPSO 532 nm total

attenuated backscatter coefficients. The difference between the backscatter coefficients for molecular scattering and those for clouds and aerosols formed the basis for differentiation. Random noise in the lidar signal and the tenuous nature of thin clouds made the detection difficult. Vertical and horizontal averaging were used in order to increase the signal-to-noise ratios for detection [*Winker et al.*, 2010; *Vaughan et al.*, 2010]. Between 8.2 km and 20 km the averaged grid squares represented a 15 km horizontal (15 profiles with 1 km horizontal resolution in the backscatter coefficients at this altitude range) and 240 m (4 adjacent levels) vertical averages. There were 150 lidar profiles for each 50 km region giving 10 averaged horizontal grid squares across the region and 49 averaged squares between 8.2 and 20 km. If the difference in the averaged 532 nm total attenuated backscatter coefficient between two vertically adjacent grid boxes exceeded 0.0031 km^{-1} sr^{-1}, then the existence of a cirrus cloud was deemed possible and the scene was not analyzed. The difference between backscatter coefficients for cloud-free air above 8.2 km in two vertically adjacent grid boxes is typically less than 0.003 km^{-1} sr^{-1}. The probing was done vertically in search of thin clouds with cloud-free air above and below the clouds. When the backscatter coefficient exceeded the threshold, visual inspection of images constructed from the backscatter coefficients usually revealed that a cloud was present. The grid averaging strategy was applied to limit the number of regions falsely identified as containing cirrus clouds when no averaging was applied. With no averaging, false positives were frequent in regions under the high levels of background noise typical of daytime observations. An examination of rejected scenes indicated that the cirrus filter performed well most of the time. In this study the objective was to eliminate even the weakest indications of thin cirrus in order to avoid the effects such clouds might have on the retrieved properties for the low-level marine stratocumulus.

[12] A second filter was developed to detect midlevel clouds between 5 km and 8.2 km in order to ensure that the regions analyzed contained no clouds other than a single-layered, low-level, marine cloud system. The vertical resolution of the CALIPSO backscatter coefficients is 30 m below 8.2 km. A running average over three vertical bins (90 m) and 15 profiles (5 km) between 5 and 8.2 km was implemented along the orbit. If the average attenuated 532 nm backscatter coefficient exceeded 0.01 km^{-1} sr^{-1}, then the presence of a midlevel cloud was deemed possible and the scene was excluded from analysis.

2.3. Identification of Marine Stratus and Stratocumulus in the CALIPSO Lidar Data

[13] For 50 km segments that passed the cirrus and midlevel cloud filters, a low-level marine stratus cloud detection routine was used to identify each lidar profile as either overcast, partly cloudy, or cloud free. The low-level cloud detection scheme operated on the full resolution (30 m vertical, 333 m horizontal) 532 nm total attenuated backscatter coefficients beginning at 5 km and ending 100 m above the surface. The 100 m cutoff was chosen to avoid difficulties associated with detecting near-surface layer clouds or fog. Following *Mahesh et al.* [2004], cloud detection required at least three vertical bins to exceed a threshold value. For this study, additional criteria had to be met to ensure that a detected cloud had some degree of horizontal and vertical continuity. The 532 nm total attenuated backscatter coefficient in a single profile had to exceed a threshold of 0.05 km^{-1} sr^{-1} for three adjacent vertical levels. Below 5 km this threshold is considerably larger than the average molecular backscatter of 0.0013 km^{-1} sr^{-1} and noise 0.006 km^{-1} sr^{-1}. Also, the backscatter coefficients at the same vertical levels were required to exceed the threshold in at least two horizontally adjacent profiles. Once these criteria were met a cloud top was identified at the altitude of the first instance that the threshold was exceeded. The criteria for the vertical and horizontal continuity of the cloud signal were chosen to avoid the misidentification of noise spikes as clouds. The cloud detection routine appeared to perform well when compared with the visual inspection of images constructed from the backscatter coefficients. Jumps in cloud altitude that were greater than 0.5 km between adjacent profiles were taken to indicate the existence of multiple cloud layers. Regions with such discontinuities were not included in the analysis. Comparison of the altitudes derived using this detection scheme and those obtained from the CALIPSO level 2 cloud product will be presented in section 3.

[14] When the ocean surface was detected in a lidar profile, the clouds detected in the same profile were taken to be either optically thin or broken. Typically, three lidar profiles were collocated with each MODIS pixel. For the purposes of this study, MODIS pixels in which the cloud layer was detected and for which any of the collocated lidar profiles detected the surface were taken to be "partly cloudy." The surface was often detected near the edges of cloud layers, presumably where the clouds became thin. The threshold used in this study to identify the surface was a 532 nm total attenuated backscatter coefficient that exceeded 0.025 km^{-1} sr^{-1} below 100 m. The threshold for surface detection is smaller than that used for clouds in order to account for the attenuation of the lidar beam as it passes through clouds.

[15] A 50 km segment was taken to be overcast if all CALIPSO profiles along the segment detected a low-level cloud but no underlying surface. A segment was identified as containing a layer of broken clouds if a single, low-level cloud layer was detected in at least 30% of the profiles and there were at least three "breaks" of at least one lidar profile each that contained cloud-free air to the surface. The breaks had to fall between lidar profiles in which the cloud layer was detected. The absence of a detected cloud itself was not sufficient to label the profile as cloud free. A cloud-free profile or "break" was identified if the 90 m vertical average of the 532 nm total attenuated backscatter coefficient was less than 0.01 km^{-1} sr^{-1}. This threshold is substantially smaller than the threshold used to detect clouds but larger than the average noise level between 100 m and 5 km. It also allowed for scattering by aerosols. A smaller threshold would have resulted in many profiles with greater than average noise or aerosol concentrations to fail the cloud-free threshold, resulting in fewer broken cloud segments qualifying for further analysis. The 50 km segments with fewer than three cloud-free breaks were not analyzed.

2.4. Analysis of Collocated MODIS Observations

[16] Parameters of interest for this study included cloud layer temperature, visible optical depth, and droplet effective radius derived using the 1.6, 2.1, and 3.7 μm reflectances. The

Table 1. Number and Percentage of 50 km Regions That Survived Successive Data Screening Tests[a]

Screening	Number	Percentage
Fifty kilometer regions identified as containing marine stratus or stratocumulus based on MODIS observations	6353	100
Regions identified as low-level, single-layered on the basis of CALIPSO analysis of the 50 km segment within the regions	5574	87.7
Regions in which the cloud layer was detected in at least 30% of the lidar profiles in the region	3203	50.4
Regions identified as overcast (marine stratus)	1566	24.6
Regions in which at least 50% of the MODIS pixels yielded valid MOD06 and partly cloudy pixel retrievals	1561	24.6
Overcast regions in which the underlying surface was not detected in any of the lidar profiles	660	10.4
Regions identified as containing broken clouds (marine stratocumulus)	1637	25.8
Regions in which at least 50% of the MODIS pixels yielded valid MOD06 and partly cloudy pixel retrievals	1570	24.7
Regions in which at least five overcast and five partly cloudy pixels yielded valid MOD06 or partly cloudy pixel retrievals collocated with the CALIPSO lidar	574	9.0

[a]Percentages are based on 6353 50 × 50 arrays of 1 km MODIS pixels identified as containing a low-level, single-layered system of marine stratus or stratocumulus through the application of partly cloudy pixel retrievals and statistical tests to the radiances of 1017 MODIS granules from 127 days of observations between 13 June and 31 October 2006.

cloud properties were obtained for the MODIS pixels collocated with the CALIPSO lidar beam and at least 50% of the pixels within a 50 km segment had to have valid MODIS MOD06 and partly cloudy pixel retrievals.

[17] CALIPSO cloud top temperatures were inferred from CALIPSO detected cloud altitudes using the coincident temperature profiles generated by NASA's Global Modeling and Assimilation Office (GMAO) and included as part of the CALIPSO level 1 data. Errors in analyzed meteorological fields are expected over sparsely observed ocean regions. Discrepancies of as much as a couple of degrees between the analyzed and radiosonde estimates of inversion temperatures associated with low-level marine stratus and stratocumulus have been documented [*Wood and Bretherton*, 2006]. In addition, *Holz et al.* [2008] have discussed algorithmic issues with the MOD06 cloud product that, on the basis of the analyzed temperature profile, places low-level marine stratus as much as a kilometer above the actual altitude. Such errors were encountered in this study. To avoid such errors, only the departures of the layer temperatures from their overcast means within 50 km segments were compared. Similarly, departures of cloud optical depths and droplet radii from the means of the overcast pixels within each segment were compared. For the overcast segments, the variations in the cloud properties were from the means of all the pixels. For segments with broken clouds, variations of temperature, optical depth, and droplet radius were determined for both the overcast pixels and the partly cloudy pixels. For the partly cloudy pixels, the variations were determined by subtracting the values for pixels collocated with CALIPSO lidar profiles in which no surface was detected (overcast) from the means of pixels collocated with profiles in which the surface was detected (partly cloudy).

3. Results

[18] A total of 6353 50 × 50 arrays of MODIS pixels identified as containing a single-layer system of marine stratus or stratocumulus on the basis of the application of partly cloudy pixel retrievals and additional statistical tests applied to the MODIS radiances were found in 1017 MODIS granules, each granule accounting for 5 min of an orbital segment. Table 1 shows the number of regions that passed subsequent scene identification and cloud layer tests. Following the application of the multilayer cloud filters, 87.7% of these regions were deemed single layered. At least 50 lidar profiles within a region were required to have detected a cloud layer for the region to be analyzed further. Only 50.4% of the initial 50 km regions identified using the MODIS observations had sufficient cloud cover to meet this requirement. Of the 2371 regions that lacked a sufficient number of CALIPSO cloud layer detections, 75.7% (1795) had no clouds detected at all and could be considered "cloud free." A sizable fraction of the regions identified as having a single layer of clouds on the basis of the MODIS data failed a matching identification on the basis of the CALIPSO observations. Evidently, the path of the lidar beam fell in cloud-free portions of the 50 km scale regions. The cloud top detection routine was capable of detecting clouds with visible optical depths of approximately 0.1. Such clouds might be attributed to cloud contamination in otherwise cloud-free pixels or as aerosols in the operational MODIS processing. The 50 km segments that met all criteria for low-level, single-layered systems were then labeled as "overcast" if all CALIPSO profiles revealed the presence of a single cloud layer with no evidence of the underlying ocean surface. Segments were identified as containing "broken clouds" if fewer than 150 of the lidar profiles in the region detected the cloud layer and at least three of the profiles were identified as being cloud free to the surface. To assess the relationships predicted by adiabatic cloud parcel models, additional requirements were imposed. The broken cloud regions had to have at least 5 overcast and 5 partly cloudy pixels for which valid cloud properties were obtained from either the MOD06 cloud product or the partly cloudy pixel retrievals. The additional criteria improved the stabilities of the average cloud properties for both the overcast and the partly cloudy pixels.

3.1. Comparison of CALIPSO-Derived Cloud Top Altitudes

[19] Cloud heights derived using the cloud top detection scheme (CTDS) produced altitudes that compared well with

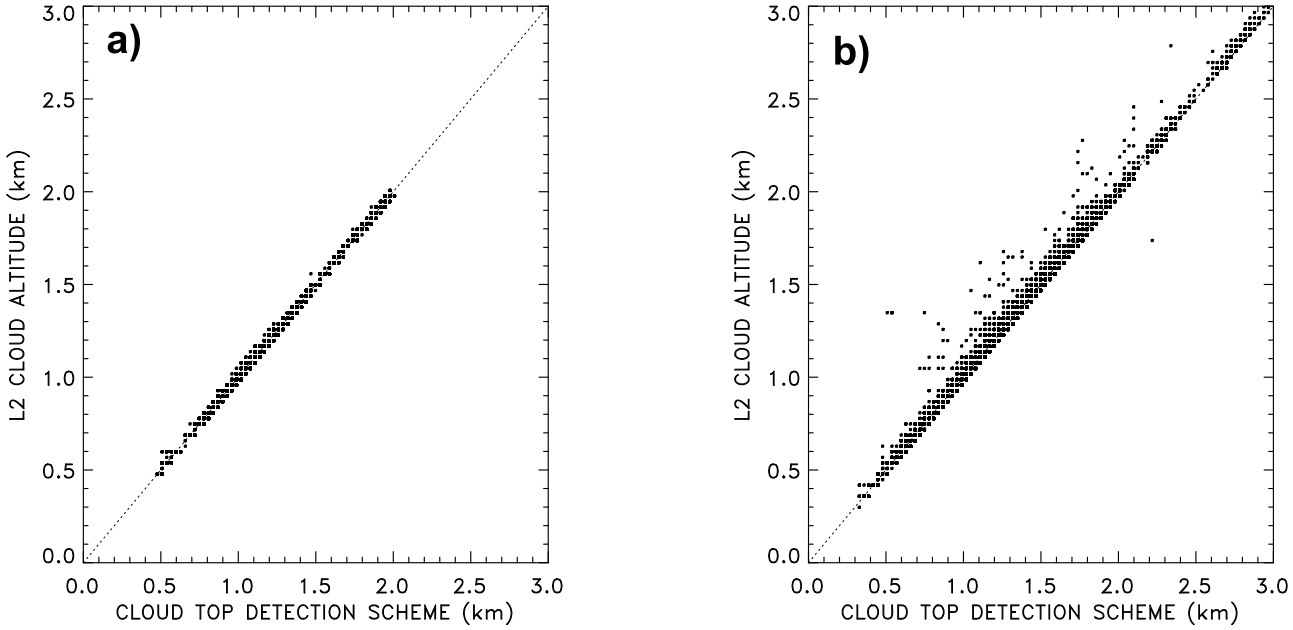

Figure 2. Cloud altitudes derived for low-level marine clouds using the cloud top detection scheme developed for this study and those obtained from the CALIPSO level 2 cloud product for 50 km ocean regions in which returns were obtained only from (a) a single layer of marine stratus and no surface returns were detected and (b) both a single layer of marine stratocumulus and the underlying surface.

those in the CALIPSO level 2 data products. Figure 2 shows CTDS and the CALIPSO level 2 altitudes for seventy-eight 50 km segments that were overcast and 221 segments that had broken, low-level, single-layered clouds. Only the altitudes for lidar profiles with returns from both the cloud layer and the surface are shown for the broken cloud segments. Clearly, the altitudes obtained with the CTDS were well correlated with the CALIPSO level 2 cloud altitudes. The average for the overcast segments placed the CTDS altitudes 1 m above the level 2 altitudes with a standard deviation of about 20 m. For broken clouds, the CTDS altitudes were 5 m below the level 2 altitudes with a standard deviation of 35 m. Departures of the CTDS from the CALIPSO level 2 altitudes typically fell within the adjacent 30 m altitude bin.

[20] The CALIPSO level 2 cloud identification scheme was more sensitive to thin clouds than the CTDS developed for this study. The higher sensitivity was reflected in the higher altitudes detected in the case of broken clouds, as shown in Figure 2, and in the frequencies of cloud detection shown in Table 2 for the profiles in which both a cloud layer and the surface were detected using either method. The level 2 and the CTDS agreed on all overcast profiles (no underlying surface detected). In nearly 17% of the CALIPSO profiles in which both a low-level cloud layer and the surface were detected, a layer was detected by the level 2 algorithm but no cloud was detected using the CTDS. For comparison, in only 2% of the profiles did the CTDS identify a cloud layer not reported by the CALIPSO level 2 algorithm. The additional sensitivity of the level 2 algorithm arises in part from (1) accounting for the attenuation of the lidar beam by layers above the cloud, (2) averaging vertically and horizontally to improve the signal-to-noise ratios for cloud detection, and (3) using a dynamic threshold that accounts for molecular scattering as opposed to the fixed threshold in the CTDS.

3.2. Fractional Cloud Cover in the 1 km MODIS Pixels

[21] Partly cloudy pixel retrievals were used to determine the cloud fraction in pixels associated with CALIPSO lidar profiles in which the cloud layer was detected but the underlying surface was not (overcast) and profiles in which both clouds and the underlying surface were detected (partly cloudy). Figure 3 shows the pixel-scale distributions of fractional cloud cover for pixels associated with overcast and broken clouds as deduced from the CALIPSO lidar returns. Owing in part to the requirements described in section 3.1, that each 50 km region analyzed had to have a single layer of low-level cloud and that within the associated 50 km segment the layer had to be detected in at least one third of the lidar returns, overcast 1 km MODIS pixels dominated the population. In addition, the procedures used to estimate layer altitudes in the partly cloudy pixel retrieval scheme rely on the occurrence of overcast pixels in the

Table 2. Cloud Detection Frequencies for the CTDS and CALIPSO Level 2 Cloud Product for Lidar Profiles Within 50 km Segments Containing Broken Clouds in Which Both the Cloud Layer and the Underlying Surface Were Detected[a]

		CTDS	
CALIPSO L2		No Cloud (%)	Cloud (%)
No Cloud (%)	34.32(3052)	**31.85**(2864)	2.091(188)
Cloud (%)	66.06(5941)	16.74(1505)	**49.33**(4436)
Total	100(8993)	48.58(4369)	51.42(4624)

[a]Percentages in bold indicate agreement between the CTDS and CALIPSO level 2 detection routines. Numbers in parentheses give the number of lidar profiles involved.

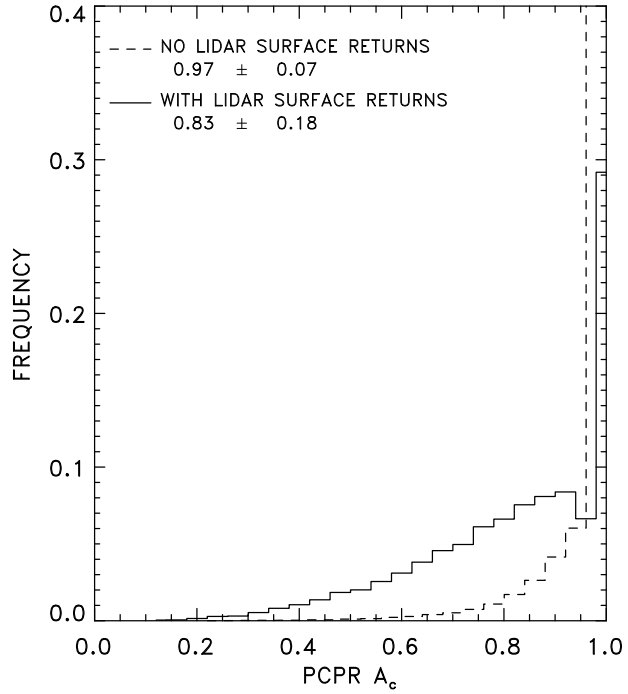

Figure 3. Pixel-scale cloud fraction derived using partly cloudy pixel retrievals (PCPR) for 1 km MODIS pixels collocated with the CALIPSO lidar returns in which a single-layered system of marine stratus was detected but no underlying surface was detected (dashed line) and in which a single-layered system of marine stratocumulus was detected and the underlying surface was also detected (solid line). Observations were taken from 50 km scale regions that were overcast and regions that contained broken clouds. For the ensemble of regions analyzed, the frequency of overcast pixels with no surface lidar returns is 0.82.

vicinity of the region being analyzed. As a result, retrievals are performed most frequently for regions that are mostly cloudy, and because of their lack of overcast pixels, rather infrequently for regions with sparse cloud cover [*Coakley et al.*, 2005]. Consequently, the distribution of pixel-scale fractional cloud cover in this study is skewed toward large cloud fractions. MODIS pixels identified as overcast by the CTDS had an average fractional cloud cover of 0.97 ± 0.07. Of the pixels identified as overcast, 82% were also identified as overcast by the partly cloudy pixel retrievals. Pixels associated with a CALIPSO lidar profile in which both the cloud layer and the underlying surface were detected had an average fractional cloud cover of 0.83 ± 0.18. Of these pixels, 55% had retrieved cloud cover fractions smaller than 0.9. Despite the prevalence of overcast conditions, a sizable number of MODIS pixels were included for which the retrieved cloud cover fraction was well below unity. Such pixels are treated as overcast in the creation of the MOD06 cloud product. The overcast assumption leads to biases in the retrieved cloud layer temperature, optical depth, and droplet radius, as discussed in sections 3.3–3.5.

3.3. Visible Optical Depths

[22] Figure 4 shows visible optical depths obtained from the MOD06 cloud product and from the application of the partly cloudy pixel retrieval scheme. Results are separated into those for pixels found to be overcast on the basis of the analysis of the CALIPSO 532 nm total attenuated backscatter coefficients (no underlying surface detected) and those found to contain broken clouds (underlying surface detected). For overcast pixels the partly cloudy pixel retrievals gave slightly larger visible optical depths than found in the MOD06 cloud product. The larger optical depths arise in part from the assumption of zero surface albedo in the partly cloudy pixel retrievals as opposed to an albedo of 0.05 to account for the diffuse reflectance from the underlying ocean in the MOD06 retrievals [*Platnick and Oreopoulos*, 2008]. The difference in surface albedos accounts for 30–50% of the differences in the retrieved optical depths, with the larger percentages occurring for the smaller optical depths. The remaining differences are probably caused by the differences in the two retrieval schemes: different atmospheric profiles, different radiative transfer models, and different numerical schemes for obtaining the retrieved properties. As would be anticipated given the detection of the surface, the optical depths in pixels containing broken clouds were much smaller than those in the overcast pixels. Figure 5 shows the optical depths for MODIS pixels identified as being overcast by the partly cloudy pixel retrieval but for which the underlying surface was detected in a collocated lidar return. For the range of visible optical depths encountered in this study, approximately 5 to 20, the fractional change in the reflectance at 0.64 μm for a unit change in optical depth is linearly proportional to the fractional change in the optical depth and the coefficient of proportionality is nearly constant. Thus, the fractional difference between the MOD06 and partly cloudy pixel retrieval optical depths shown in Figure 4 for overcast pixels with an optical depth of 10 is 17% and that in Figure 5 for optical depth of 5 is 20%. For the differences between the MOD06 and partly cloudy pixel retrieval optical depths for the broken clouds shown in Figure 4; however, the fractional change is much larger, greater than 50%. The larger change for the partly cloudy pixels is the result of accounting for the partial filling of the pixels by clouds in the partly cloudy pixel retrievals as opposed to assuming that the pixel is overcast as in the MOD06 retrievals.

[23] Interestingly, the results in Figure 5 also show that regardless of which retrieval was used, the surface was detected even for clouds with pixel-scale optical depths as large as 10, for which the lidar beam should have been attenuated. The detection of the surface for such clouds suggests that while the average pixel-scale optical depth may have been large, sufficient variability in liquid water amounts within the pixels allowed the lidar beam to penetrate through optically thin portions. In some cases, however, the lidar returns found cloud-free holes. Of the MODIS pixels identified as overcast by the MOD06 processing and for which the underlying surface was detected in a collocated lidar return, 16% had at least one of the collocated lidar returns indicating cloud-free conditions. Of this 16%, only 14% were identified as overcast by the partly cloudy pixel retrieval scheme. The remaining 86% were identified as partly cloudy with an average cloud cover fraction of 0.23.

3.4. Optical Depth and Cloud Temperature Variations

[24] For the MODIS pixels collocated with the CALIPSO lidar beam, departures of the 1 km pixel-scale cloud optical

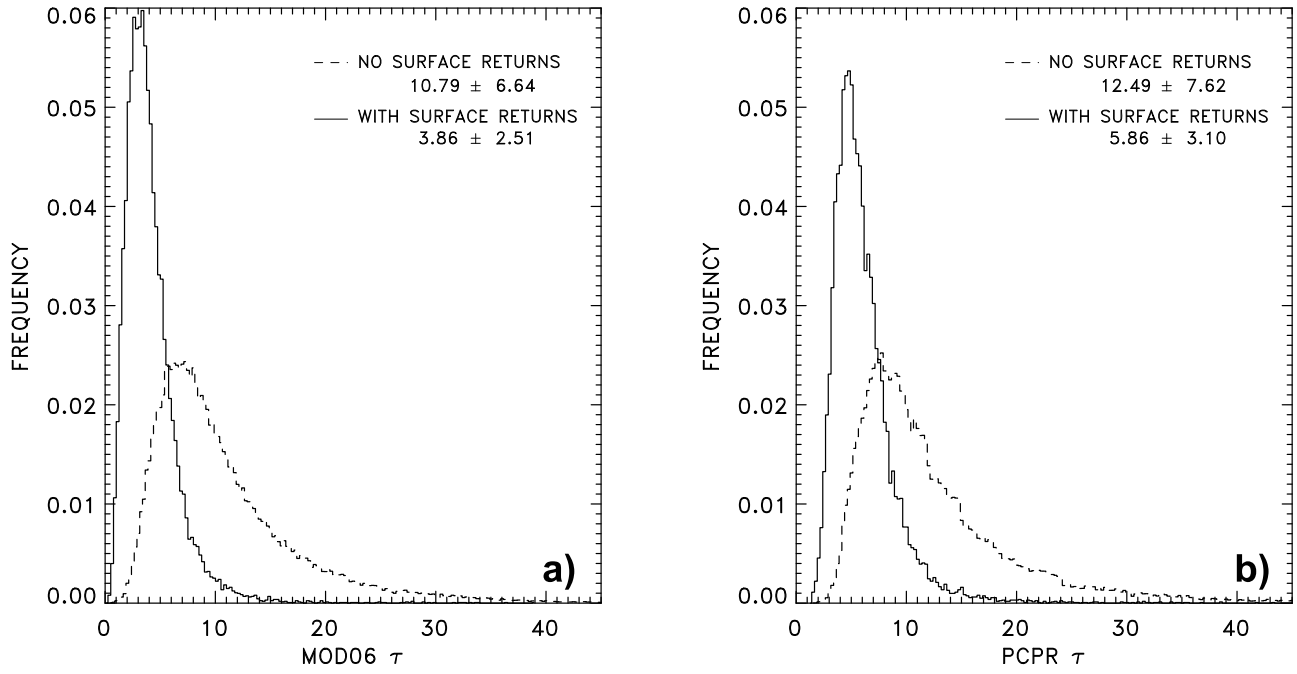

Figure 4. Optical depths from (a) the MODIS cloud product and (b) partly cloudy pixel retrievals for 1 km MODIS pixels, in which there were lidar returns from a single-layered system of marine stratus and the surface was not detected (dashed line), and for pixels in which both the cloud layer and the surface were detected (solid line).

depths from the averages for the overcast means within the 50 km segments were analyzed together with the departures of the cloud layer temperatures from the overcast means. The departures in temperatures obtained for the CALIPSO lidar profiles were derived from the departures in the cloud top altitudes and the analyzed temperature lapse rates at that level provided in the CALIPSO data. For 50 km segments that contained overcast pixels, the departures were from the averages of all pixels within the segment. For 50 km segments that contained broken clouds, the departures were from the averages of pixels identified as being overcast within the segment (no underlying surface detected in the lidar backscatter coefficients).

[25] Figure 6 shows the distribution of optical depth and temperature departures for 50 km segments derived using the CALIPSO lidar backscatter coefficient and the MOD06 cloud product. Figure 7 shows the same distributions derived using partly cloudy pixel retrievals. In Figures 6 and 7 the relative frequencies were obtained by binning the departures of optical depth, $\Delta\tau$, in bins with a width of 0.125 over the range −15 to 15. The departures in temperature, ΔT_c, were distributed in bins of 0.25 K in width over the range −3 to 3 K. Only bins with at least 5 occurrences are displayed in Figures 6 and 7. For overcast 50 km segments, the MOD06 and partly cloudy pixel retrieval departures were similar. The range of temperature variability for the MOD06 product and the partly cloudy pixel retrievals were similar to that deduced from the CALIPSO lidar backscatter coefficient. The slightly larger variability exhibited by the MOD06 temperature departures results from reporting the temperatures of the sounding levels associated with the analyzed profiles that are nearest the observed 11 μm emission temperatures as opposed to simply reporting the emission temperatures. For the partly cloudy pixels, the MOD06 cloud product showed behavior expected of the overcast assumption used to analyze the radiances. The optical depths were smaller than those of the nearby overcast pixels and the cloud

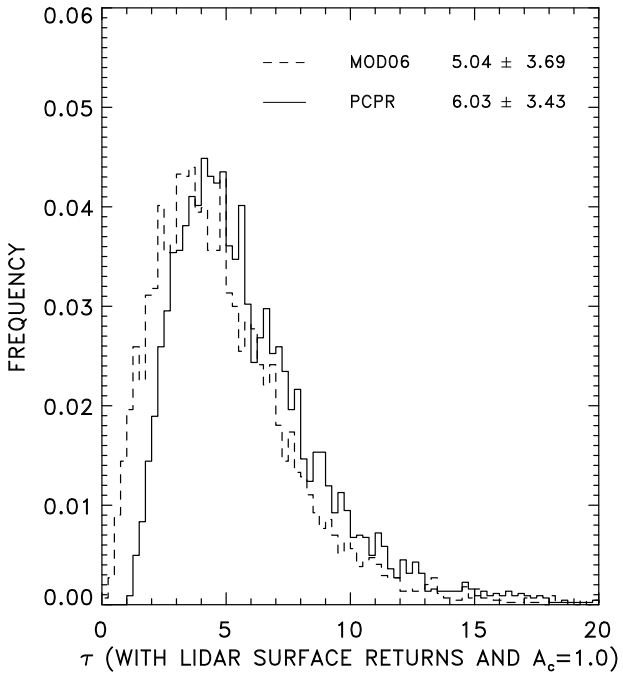

Figure 5. Optical depths for pixels identified as overcast by the partly cloudy pixel retrievals and were collocated with a CALIPSO lidar profile in which the surface was detected.

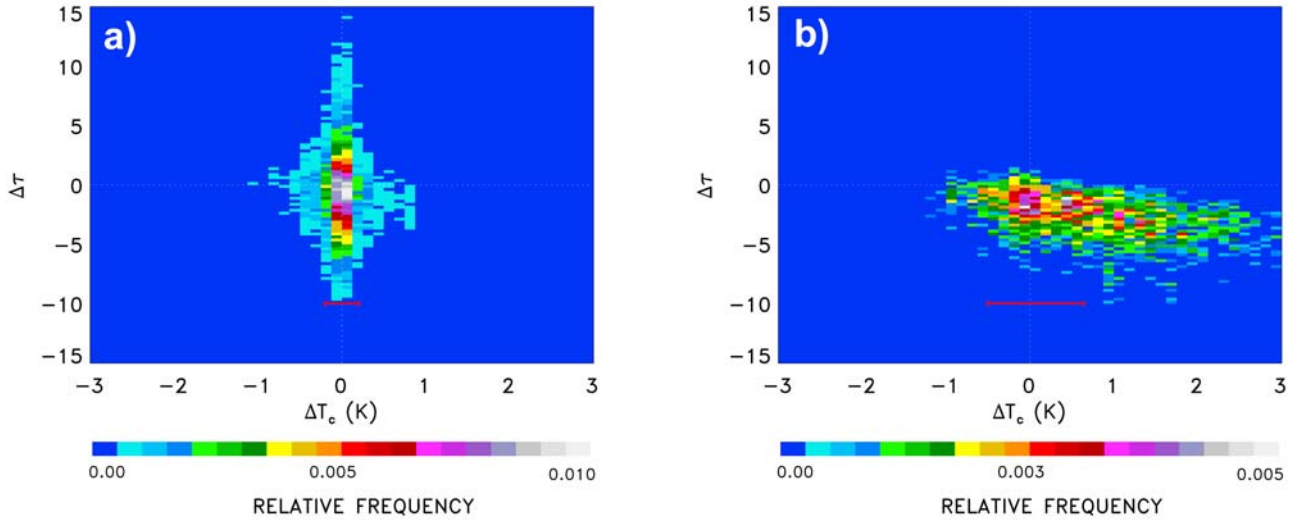

Figure 6. Departures of optical depth and cloud layer temperature from the means of the overcast pixels as obtained from the MODIS cloud product for (a) 50 km segments in which no underlying surface was detected in the lidar returns and (b) for pixels in which both the cloud layer and the underlying surface were detected. The error bar plotted below the distribution gives ± 1 standard deviation of temperature departures derived from the CALIPSO lidar returns for the associated MODIS pixels.

layer temperatures were higher than would be inferred from the range of altitudes derived from the CALIPSO lidar backscatter coefficient. However, while the optical depths derived using the partly cloudy pixel retrievals were likewise smaller than those of the clouds in nearby overcast pixels, the range of temperatures was comparable to that inferred for the CALIPSO observations. Of course, in the partly cloudy pixel retrievals, the pixels not overcast by the cloud layer were assumed to be at the same altitude as the clouds in the nearby overcast pixels. The temperature range derived from the CALIPSO data appears to support this assumption. In addition, CALIPSO lidar returns were used to determine the differences between the altitudes for MODIS pixels containing broken clouds and those in the overcast pixels within the 50 km segments. The average difference was −0.001 ± 0.03 km (mean ± standard deviation).

3.5. Droplet Radius and Cloud Temperature Variations

[26] Figure 8 shows distributions of temperature and droplet effective radius departures for 50 km segments. The droplet radii were derived using reflectances at 2.1 μm. Figure 8 shows the departures derived using the CALIPSO lidar backscatter coefficient and the MOD06 cloud product. Figure 9 shows the same distributions derived using the partly cloudy pixel retrieval scheme. In Figures 8 and 9 the

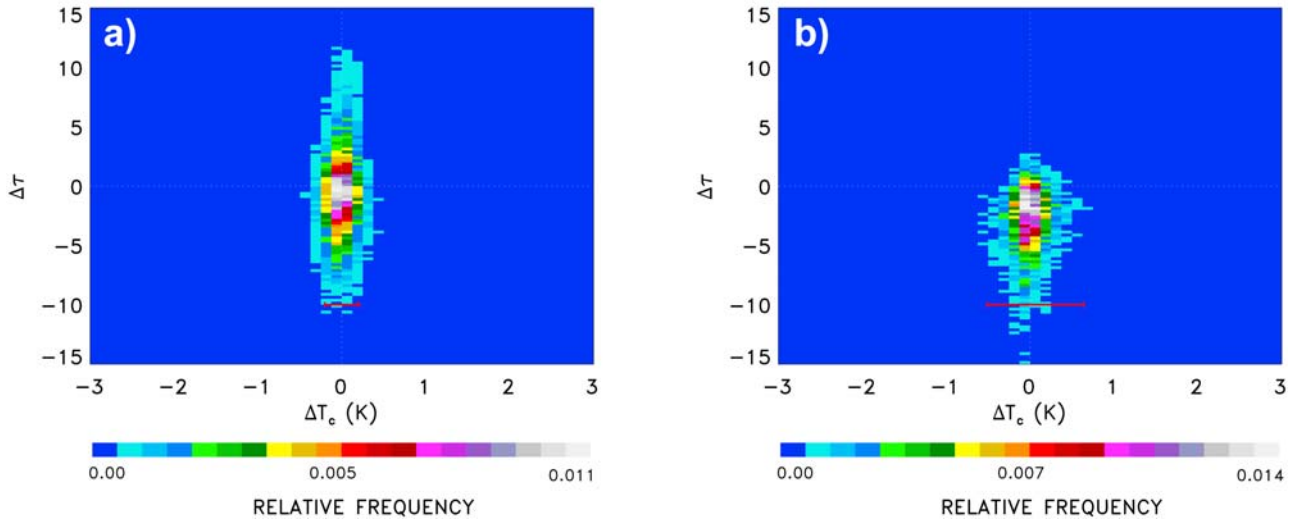

Figure 7. Same as Figure 6 but for optical depths and cloud layer temperatures derived from partly cloudy pixel retrievals.

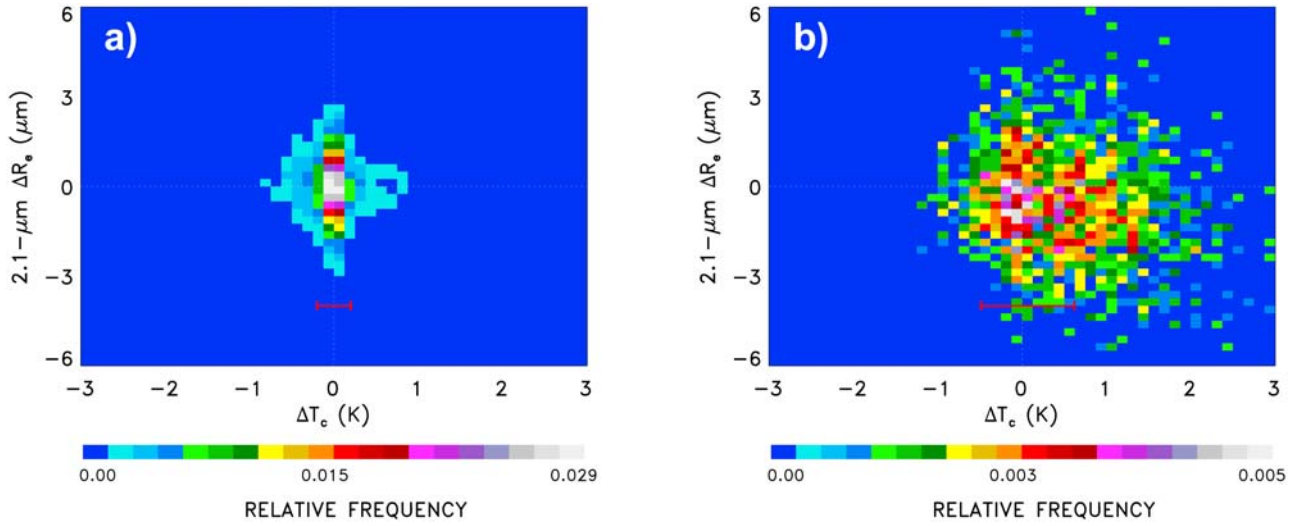

Figure 8. Same as Figure 6 but for 2.1 μm derived droplet effective radius and cloud layer temperature derived from the MODIS cloud product.

relative frequencies were obtained by binning the departures in temperature as done previously and binning the departures in droplet radius, ΔR_e, in bins with widths of 0.25 μm for the range −6 to 6 μm. Aside from the greater variation in layer temperature for the MOD06 cloud product noted previously, for the overcast 50 km segments the MOD06 and partly cloudy pixel retrievals produced similar results. For the pixels containing broken clouds, the MOD06 cloud product showed behavior expected for the application of the overcast assumption to partly cloudy pixels. Many, but not all, of the droplet radii for the pixels containing broken clouds were 1–2 μm larger than those derived for the pixels identified as being overcast. When a pixel is only partially cloud covered, the reflectances at both the visible and near infrared wavelengths are generally smaller than those for overcast pixels. Thus, while the retrieved optical depth is underestimated, it could nonetheless be sufficiently large as to suggest that the cloud is nearly opaque at 2.1 μm. The low reflectance in the near infrared, however, suggests that the droplet effective radius is relatively large. When the pixel fractional coverage is relatively small, so that the retrieved optical depth indicates that the cloud is semitransparent at 2.1 μm, the retrieved droplet radii can either be larger or smaller, depending on optical depths and cloud fractions, than those for the clouds in the overcast pixels.

[27] The results in Figures 8 and 9 reveal that the departures in the retrieved radii obtained with the partly cloudy pixel retrievals had distributions nearly identical to those obtained with the MOD06 cloud product, even for pixels that were identified as being partly cloud covered. This result was unexpected. When the retrieved cloud fraction obtained with the partly cloudy pixel retrieval scheme is used to distinguish between partly cloudy and overcast pixels, droplet radii obtained assuming that pixels are overcast when they are only

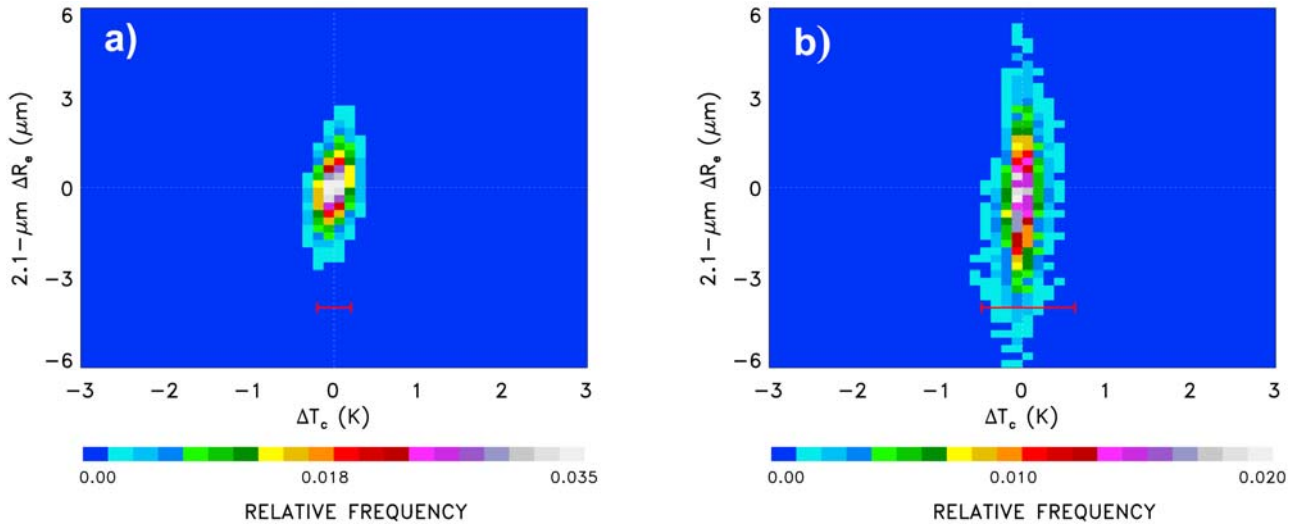

Figure 9. Same as Figure 8 but for partly cloudy pixel retrievals.

Table 3. Cloud Properties Derived From the MOD06 Cloud Product and Partly Cloudy Pixel Retrievals for Overcast and Partly Cloudy Pixels Identified Using the CALIPSO 532 nm Total Attenuated Backscatter Coefficients[a]

		Segments With Broken Clouds	
Retrieval Scheme	Overcast Segments	Overcast Pixels	Partly Cloudy Pixels
Optical Depth			
MOD06	14.11 ± 7.25	6.74 ± 5.18	3.37 ± 2.32
Number of segments	660	430	430
Partly cloudy pixel	15.71 ± 8.22	8.98 ± 6.08	5.47 ± 3.31
Number of segments	660	574	574
1.6 μm Derived Droplet Effective Radius (μm)			
MOD06	11.55 ± 3.47	13.70 ± 6.10	14.62 ± 6.86
Number of segments	646	38	38
Partly cloudy pixel	12.16 ± 3.35	14.59 ± 5.84	14.34 ± 5.80
Cloud cover	0.996	0.885	0.755
Number of segments	646	190	190
2.1 μm Derived Droplet Effective Radius (μm)			
MOD06	11.89 ± 3.34	13.71 ± 5.10	13.56 ± 5.12
Number of segments	660	430	430
Partly cloudy pixel	12.40 ± 3.29	14.22 ± 4.98	13.39 ± 5.57
Cloud cover	0.996	0.893	0.745
Number of segments	660	574	574
3.7 μm Derived Droplet Effective Radius (μm)			
MOD06	12.27 ± 3.24	13.27 ± 4.09	12.39 ± 4.04
Number or segments	659	367	367
Partly cloudy pixel	12.59 ± 3.60	13.47 ± 4.78	11.84 ± 4.38
Cloud cover	0.996	0.892	0.748
Number of segments	659	558	558

[a]The results are for 50 km segments that were overcast by marine stratus and segments in which there were breaks in the cloud layer.

partly cloudy are typically 1 μm to 2 μm larger, depending on the regional cloud cover, than those for the pixels identified as overcast within the same 50 km scale region. Here, the lidar 532 nm total attenuated backscatter coefficients rather than the pixel-scale cloud fraction were used to identify pixels as either overcast or partly cloudy. As shown in Figure 3, 29% of the pixels identified as partly cloudy on the basis of the backscatter coefficients had retrieved pixel-scale cloud fractions indicating that they were overcast. For these pixels, the droplet radii obtained from the MOD06 cloud product and partly cloudy pixel retrievals were nearly the same. For the remaining 71% of the partly cloudy pixels, the majority had cloud cover fractions greater than 0.8. As a result, the average of the retrieved droplet radius for the partly cloudy pixels differed little from those identified as overcast. In addition, as shown in Figures 4 and 5, the optical depths of the partly cloudy pixels that were identified as overcast on the basis of the cloud cover fraction had optical depths that were nearly half those of the pixels identified as overcast on the basis of the lidar backscatter coefficients. Many of these clouds were semitransparent at 2.1 μm thereby giving rise to influences caused by variations in liquid water amounts and droplet radii within the MODIS pixels. For much the same reasons that the overcast assumption applied to partly cloudy pixels produces droplet radii that are larger than those for nearby overcast pixels, variations of liquid water amount and droplet radii within pixels that are semitransparent at the near infrared wavelength can lead not only to underestimates of the average optical depth but also to overestimates of the average droplet radius. The combination of the subpixel-scale variations and the large overlap between pixels identified as partly cloudy using the lidar backscatter coefficients but having retrieved cloud cover fractions near unity are thought to explain the similarity in the distributions of droplet radii obtained for the MOD06 and partly cloudy pixel retrievals.

[28] Table 3 provides additional evidence suggesting that subpixel-scale variability may lead to behavior in the retrieved cloud properties that is similar to that for partly cloudy pixels. Table 3 lists means and standard deviations of the pixel-scale optical depths and droplet effective radii derived using the 1.6, 2.1, and 3.7 μm reflectances for the 50 km segments in which all the pixels were overcast and for the 50 km segments in which there were breaks in the cloud layer. Table 3 gives the number of 50 km regions contributing segments that had the required numbers of successful retrievals for the MOD06 and partly cloudy pixel retrieval schemes. The visible optical depths listed in Table 3 are those obtained in conjunction with the retrievals of droplet radii using the 2.1 μm reflectances. The visible optical depths obtained using the 3.7 μm reflectances differed little, but owing to the defects in the Aqua MODIS detectors for 1.6 μm, relatively few retrievals were successful when using the shorter wavelength, and consequently, the associated optical depths differed slightly but noticeably from those given for the segments containing broken clouds. For the partly cloudy pixel retrievals, the fractional cloud cover of the pixels contributing to the analysis is also given in Table 3.

[29] For the segments with broken clouds, the optical depths of the pixels identified as being overcast were approximately half the optical depths in the overcast regions. The smaller optical depths might be expected given the breaks in the cloud layer. The droplet effective radii obtained with the 1.6 and 2.1 μm reflectances, however, were 10–15% larger for both the MOD06 and partly cloudy pixel retrievals. While the optical depths for the partly cloudy pixels were considerably smaller for both the MOD06 cloud product and the partly cloudy pixel retrievals, the droplet radii were comparable to those found in the overcast pixels. Only the 3.7 μm derived droplet radii retrieved for the partly cloudy pixels were substantially smaller than those for the overcast pixels within the same 50 km segments. Interestingly, as was noted by *Matheson et al.* [2006], in going from average cloud properties for 50 km regions containing broken clouds to those that are overcast, the fall in droplet radii and rise in optical depths mimic the trends expected of the aerosol indirect effect.

[30] One explanation for the larger droplets in the overcast pixels in regions containing broken clouds is droplet growth through collision and coalescence which ultimately leads to drizzle and the subsequent breakup of the layer [*Albrecht*, 1989]. The pockets of open cells and associated drizzle in marine stratocumulus described by *Stevens et al.* [2005] are examples. Another explanation is the subpixel-scale variability in liquid water amount and droplet radius mentioned earlier. In going from the overcast segments to the broken cloud segments, the percentage increases in the droplet radii derived using 3.7 μm reflectances for the overcast pixels, were less than half those obtained using the 1.6 and 2.1 μm reflectances. Absorption by liquid water is significantly larger at 3.7 μm than it is at the shorter wavelengths. Consequently, a larger fraction of the clouds in the overcast pixels and even in some of the partly cloudy pixels were likely to be opaque at 3.7 μm, thereby reducing the effects of subpixel-scale var-

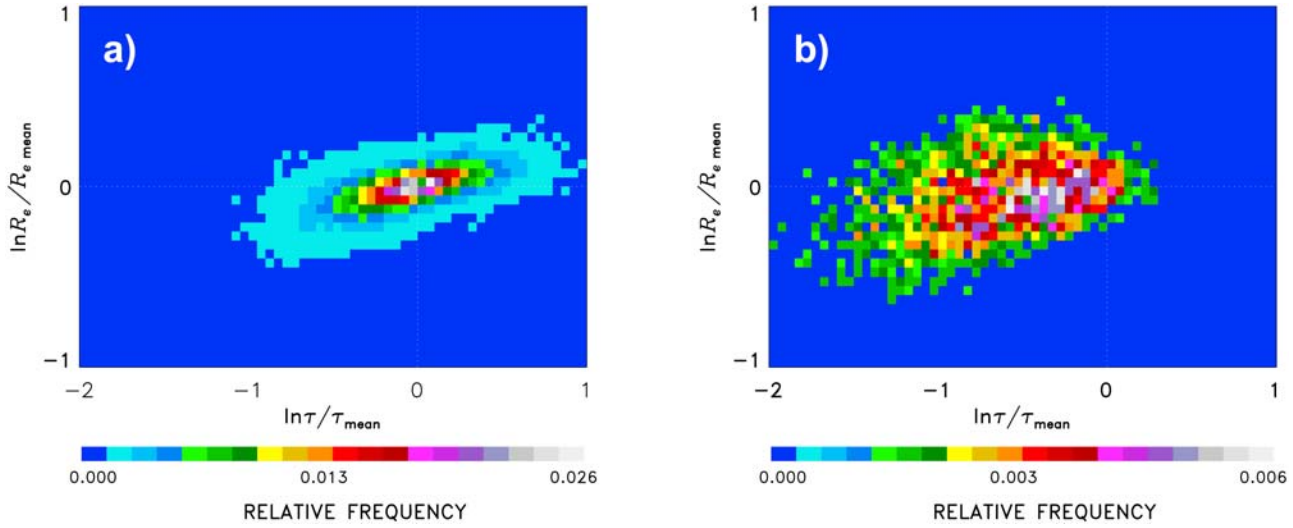

Figure 10. Departures of $\ln(R_e/R_{e\ \mathrm{mean}})$ for the 2.1 μm derived droplet effective radius and $\ln(\tau/\tau_{\mathrm{mean}})$ from zero, where the mean values are the averages of the droplet effective radii and visible optical depths for the MODIS pixels are identified as overcast. The observations are (a) for an ensemble of 50 km segments in which the MODIS pixels are collocated with the CALIPSO beam and all of the pixels were identified as overcast using the CALIPSO 532 nm total attenuated backscatter coefficients and (b) for pixels identified as being partly cloudy within an ensemble of 50 m scale segments in which there were breaks in the clouds. The cloud properties are from the MODIS cloud product.

iations in liquid water amounts. Even though the retrieved droplet radii obtained using the 3.7 μm reflectances were probably overestimated, the results in Table 3 suggest that droplets in pixels that are partly cloudy at the 1 km scale are, in fact, smaller than those in nearby pixels that are overcast.

3.6. Droplet Radius and Optical Depth Variations

[31] The relationships shown in Figures 6 and 7 and in Figures 8 and 9 suggest that the MODIS pixels identified as being overcast exhibit essentially no correlation between cloud top altitude and either optical depth or droplet effective radius. Within 50 km scale regions that contain no clouds other than a single layer of marine stratus or stratocumulus, the range of altitudes appears to be limited, perhaps by the strength of the overlying temperature inversion. Consequently, the range of variations in cloud layer temperatures within such regions is relatively small. Nonetheless, both the retrieved droplet radii and optical depths exhibit considerable variability at the 1 km scale of the MODIS pixels. Presumably, this variability is created by the variations in updrafts that lift moist air and cloud condensation nuclei to the condensation level. For adiabatic cloud parcel models, variations in optical depths and droplet radii should be related, $d\ln R_e/d\ln\tau \sim 0.2$ [*Szczodrak et al.*, 2001; *Boers et al.*, 2006]. Figure 10 shows $\ln(R_e/R_{e\ \mathrm{mean}})$ and $\ln(\tau/\tau_{\mathrm{mean}})$ within 50 km segments overcast by marine stratus (no underlying surface detected in the lidar backscatter coefficients) and for the clouds within partly cloudy pixels (both cloud and underlying surface detected in the lidar backscatter coefficients) within the segments containing broken clouds. The droplet radii were retrieved using 2.1 μm reflectances and the mean values are the averages of the droplet radii and visible optical depths of the overcast pixels within the segments. The pixel-scale values of $\ln(R_e/R_{e\ \mathrm{mean}})$ were binned in increments of 0.05 between −1.0 and 1.0 and those for $\ln(\tau/\tau_{\mathrm{mean}})$ were binned in increments of 0.05 between −2.0 and 1.0. The results in Figure 10 are for the MOD06 cloud product; those in Figure 11 are for the partly cloudy pixel retrievals. As was noted at the start of section 3, the results for broken clouds shown in Figures 10 and 11 and Tables 3 and 4 are for 50 km segments in which there were at least 5 overcast pixels (no surface detected in the lidar returns) and 5 partly cloudy pixels (surface detected in the returns).

[32] Table 4 gives the values of $d\ln R_e/d\ln\tau$ obtained for the two retrieval schemes. Values are given separately for the 50 km segments in which all of the pixels were overcast and segments in which there were breaks in the clouds. The values were obtained by performing linear least squares fits of the pixel-scale values for $\ln(R_e/R_{e\ \mathrm{mean}})$ and $\ln(\tau/\tau_{\mathrm{mean}})$ independently for each region. The values in Table 4 are the means for the regions. Also given in parentheses are the averages of the square of the correlation coefficients which provide an estimate of the fraction of the variance explained by the fits. Figure 12 shows the distributions of slopes $d\ln R_e/d\ln\tau$ derived using 2.1 μm reflectances to retrieve the droplet effective radii for overcast 50 km segments, for overcast pixels in 50 km segments with breaks in the clouds, and for partly cloudy pixels in the segments with broken clouds.

[33] For the 50 km segments in which all of the pixels were identified as overcast, $d\ln R_e/d\ln\tau$ for the 2.1 μm derived droplet effective radii were close to that expected from adiabatic cloud parcel models, 0.20 for the MOD06 retrievals, and 0.18 for the partly cloudy pixel retrievals. As the results in Figure 12 show, though broadly peaked near the expected value, the distribution of the slopes spans a domain ranging

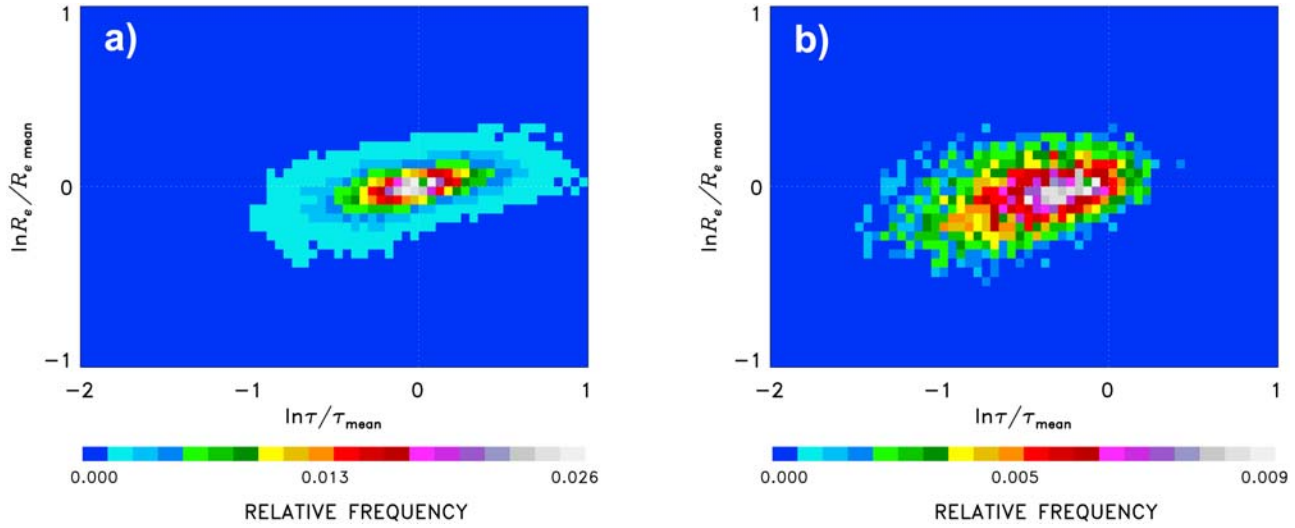

Figure 11. Same as Figure 10 but for the partly cloudy pixel retrievals.

from −0.2 to 0.6. Similar results were obtained using the 3.7 μm derived droplet effective radii and are consistent with those obtained by *Eitzen et al.* [2008]. Eitzen et al. used the MODIS 3.7 μm reflectances to derive droplet radii and reported findings for regions of shallow cumulus, which they defined as having 10–40% cloud cover, stratocumulus, 40–99% cloud cover, and overcast, 99–100% cloud cover. As indicated in Table 4, the fits obtained using the 1.6 μm derived droplet effective radii were substantially worse than those obtained using the longer wavelengths, possibly because fewer than 60% of the MODIS pixels had valid 1.6 μm reflectances.

[34] The results in Table 4, as do those in Figures 10–12, also suggest that when the CALIPSO lidar returns indicated that the MODIS pixels were partly cloudy, the goodness of the least square fits suffered. With few exceptions, the values of the slopes departed markedly from that given by adiabatic cloud parcel models. Even when the fits were performed using only those pixels that were identified as being overcast, the departures were notable. Of course, even for 50 km regions overcast by marine stratus, the concept that the clouds show behavior which results from the adiabatic ascent of moist air seems dubious. Clouds in regions that are overcast often are subject to various degrees of mixing with the air aloft and substantial mixing often occurs at scales smaller than the 1 km resolution of a MODIS pixel. Likewise, some of the clouds in overcast regions could be dissipating through drizzle which would lead to departures from the conditions in adiabatic parcel cloud models. In addition, the clouds could be subject to gradients in the concentration of cloud condensation nuclei which could modify the droplet sizes so as to mask the relationships expected for adiabatic ascent. That the retrievals for the 2.1 and 3.7 μm reflectances produced relationships close to that expected of adiabatic clouds for overcast regions is perhaps remarkable. In addition, the departures of the observations from the relationships expected of adiabatic clouds for regions containing broken clouds is probably to be expected as was noted earlier [*Szczodrak et al.*, 2001; *Harshvardhan et al.*, 2004; *Schüller et al.*, 2005]. Nonetheless, the results in Tables 3 and 4 suggest that some of the discrepancies might also be caused by biases in the retrieved cloud properties.

[35] Finally, in the adiabatic ascent of moist air, droplets grow from the lifting condensation level to cloud top. Because absorption by liquid water at 3.7 μm is larger than that at 2.1 μm which in turn is larger than that at 1.6 μm, the droplet growth with increasing cloud thickness is expected to produce the largest retrieved droplet effective radii when using the 3.7 μm reflectances and the smallest when using 1.6 μm reflectances. The results in Table 3 for the overcast 50 km segments are consistent with droplets growing as the clouds thicken. The results for the segments with broken clouds, however, suggest that the largest droplets are not at the top of the cloud but deeper within the cloud. *Chang and Li* [2003] suggested that the wavelength dependence of the retrieved droplet effective radius found for the segments with broken clouds might indicate the presence of drizzle in the lower layers of the clouds. Such behavior appears to occur in continental clouds, like those they studied, but has not commonly been observed in aircraft observations

Table 4. The $d\ln R_e/d\ln\tau$ and Fraction of Variance Explained by Least Squares Fits Derived From the MOD06 Cloud Product and Partly Cloudy Pixel Retrievals for Overcast and Partly Cloudy Pixels Identified Using the CALIPSO 532 nm Total Attenuated Backscatter Coefficients[a]

Retrieval Scheme	Overcast Segments	Segments With Broken Clouds	
		Overcast Pixels	Partly Cloudy Pixels
1.6 μm Derived Droplet Effective Radius (μm)			
MOD06	0.174 (0.232)	−0.009 (0.099)	0.044 (0.211)
Partly cloudy pixel	0.096 (0.205)	0.124 (0.149)	0.155 (0.236)
2.1 μm Derived Droplet Effective Radius (μm)			
MOD06	0.201 (0.452)	0.062 (0.187)	0.095 (0.237)
Partly cloudy pixel	0.177 (0.411)	0.137 (0.274)	0.197 (0.341)
3.7 μm Derived Droplet Effective Radius (μm)			
MOD06	0.188 (0.433)	0.094 (0.327)	0.099 (0.361)
Partly cloudy pixel	0.235 (0.461)	0.140 (0.291)	−0.001 (0.256)

[a]The results are for 50 km segments that were overcast by marine stratus and segments in which there were breaks in the cloud layer. The fraction of variance explained is shown in parentheses.

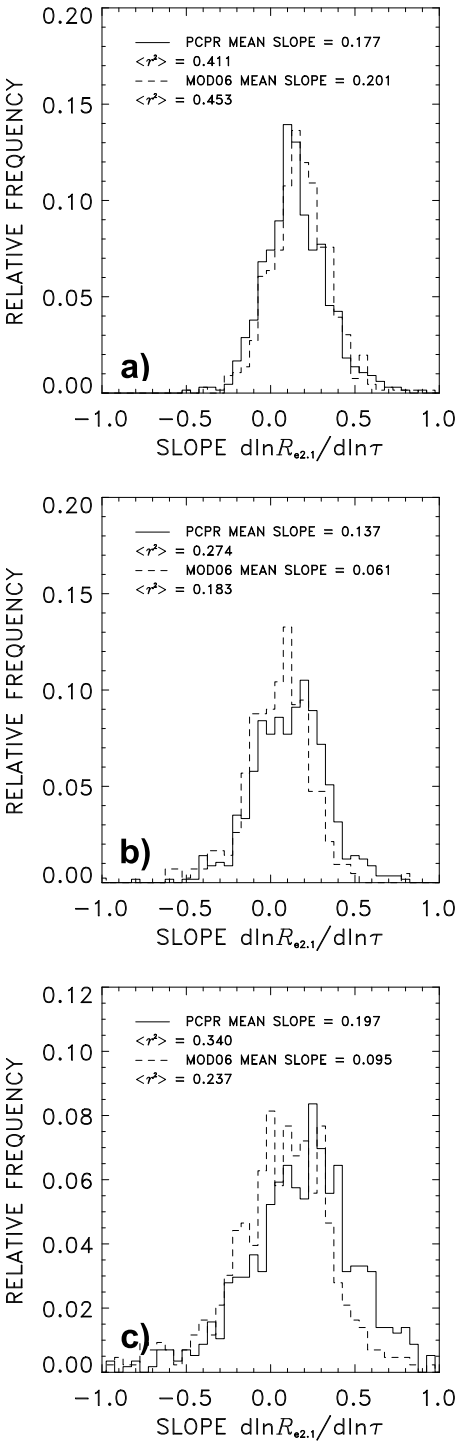

Figure 12. The $d\ln R_e/d\ln\tau$ for droplet radii derived using 2.1 μm reflectances (a) for overcast pixels in 50 km segments overcast by marine stratus, (b) for overcast pixels in 50 km segments containing broken marine stratocumulus, and (c) for the partly cloudy pixels in the segments containing broken clouds.

of marine stratocumulus [*Miles et al.*, 2000]. *Chen et al.* [2008], however, using satellite and shipboard millimeter radar, ceilometer, and microwave radiometer data, found evidence for a decrease in droplet radius with height above cloud base for marine stratocumulus undergoing moderate to heavy drizzle (>0.1 mm h^{-1}).

4. Conclusions

[36] Relationships between cloud optical depths, droplet effective radii, and cloud layer temperatures obtained from the MOD06 cloud product and a retrieval scheme that accounts for fractional cloud cover within imager pixels [*Coakley et al.*, 2005] were compared for large ensembles of 50 km scale regions that contained only a single layer of marine stratus with no breaks, or marine stratocumulus, a layer of stratus with breaks in the layer. The CALIPSO lidar 532 nm total attenuated backscatter coefficients were used to distinguish between the MODIS pixels that were "overcast," for which the underlying ocean surface was not detected in the lidar returns, and those that were "partly cloudy," for which the underlying surface was detected. The study was designed to assess whether marine stratus and stratocumulus behave as predicted by adiabatic cloud parcel models [e.g., *Boers et al.*, 2006]. Consequently, within each 50 km segment of MODIS pixels collocated with the CALIPSO lidar, departures of the cloud properties from the average values obtained for pixels found to be overcast within the segment were used to compare the relationships among the cloud properties with those predicted by adiabatic cloud parcel models. While the variations in cloud layer temperatures across 50 km regions were found to be too small to reveal any significant correlations with either the optical depths or droplet radii, strong correlations were found for the departures of the droplet effective radii with those of the optical depths. For 50 km segments in which all of the pixels were overcast, the departures in the radii and optical depths were in good agreement with the predictions of adiabatic cloud parcel models. Furthermore, the dependence of the retrieved droplet radii on the absorption by liquid water at the wavelength used to derive the droplet radii indicated that droplets grew with height above the lifting condensation level as assumed in the parcel models. For segments in which breaks were identified in the cloud layer, however, the relationships among the cloud properties departed from those predicted by parcel models for both the pixels identified as overcast and those identified as being partly cloudy. Either the conditions imposed by the parcel models failed as a result of mixing or other processes, or biases in the retrieved cloud properties that result from substantial variations of liquid water amounts and droplet radii within the MODIS pixels masked the expected outcome. These findings are consistent with the conclusions drawn by *Szczodrak et al.* [2001] and *Schüller et al.* [2005], who attempted similar assessments.

[37] The cloud properties obtained from the MOD06 cloud product and from the partly cloudy pixel retrievals agreed for the MODIS pixels found to be overcast. Variations in cloud layer temperatures within 50 km scale segments overcast by marine stratus obtained with the MOD06 and partly cloudy pixel retrievals agreed with the inferences of those variations on the basis of the variations of cloud top altitudes derived from the CALIPSO lidar and the lapse rates derived from GMAO analyzed fields. Here only departures of the layer temperatures from the means of overcast pixels within the segments were reported as the

temperatures derived from the MOD06 processing and partly cloudy pixel retrievals differed from those inferred using the CALIPSO lidar-derived cloud altitudes and analyzed temperature profiles by several degrees. Such discrepancies were probably caused by failures of the analyzed fields to capture the low-level temperature lapse rates and inversions in regions with extensive marine coverage by stratus and stratocumulus [*Wood and Bretherton*, 2006].

[38] For the partly cloudy pixels, the MOD06 optical depths and cloud layer temperatures exhibited trends expected of retrievals on the basis of the assumption that pixels in which clouds are detected are overcast. Within the regions, clouds with smaller optical depths typically had higher cloud layer temperatures, suggesting that the layer was at lower altitudes. The range of layer temperatures for the partly cloudy pixels within 50 km regions obtained from the MOD06 cloud product was considerably larger than that inferred for the CALIPSO cloud altitudes. Those derived from the partly cloudy pixel retrievals, however, were consistent with the range of CALIPSO cloud altitudes. This finding justifies the assumption underlying the partly cloudy pixel retrievals that clouds in the partly cloudy pixels within a region that contains only a single layer of clouds are at the same altitude as the clouds found in the pixels that are overcast within the region.

[39] Droplet radii retrieved for the partly cloudy pixels were found, on average, to be comparable to those of the overcast pixels within the same 50 km segments when either the 1.6 or 2.1 μm reflectances were used to retrieve the droplet radii but smaller when 3.7 μm reflectances were used. A likely cause of the larger droplets is the retrieval biases attributed to the overcast pixel approximation [*Han et al.*, 1994; *Coakley et al.*, 2005]. Interestingly, nearly identical results were obtained for the partly cloudy pixel retrievals and the MOD06 cloud products. The similarity in the results may have been caused by the large fractional cloud cover for the ensemble of cases studied. Of the pixels identified as partly cloudy on the basis of the CALIPSO 532 nm total attenuated backscatter coefficients, the partly cloudy pixel retrievals produced an average pixel-scale cloud fraction of 0.83 with 71% of the pixels having cloud fractions less than unity. In addition, for the partly cloudy pixels, the similarity of cloud properties obtained with the MOD06 and partly cloudy pixel retrievals may reflect effects owing to substantial variations in the liquid water amounts and droplet radii within pixels that are semitransparent at the near infrared wavelengths used to retrieve droplet radius. The mean optical depths of clouds in pixels found to be partly cloudy on the basis of the lidar backscatter coefficients were in many cases sufficiently small to be semitransparent in the near infrared. As absorption by liquid water is larger at 3.7 μm than at 1.6 and 2.1 μm, the retrievals obtained using the 3.7 μm reflectances are likely to be less susceptible to variations of liquid water amounts within the pixels. The fall in the 3.7 μm derived droplet radii for the partly cloudy pixels from those of nearby overcast pixels is likely to be more representative of the trend in droplet radii as cloud layers go from being overcast to broken.

[40] **Acknowledgments.** This work grew out of participation on the CALIPSO Science Team funded under NASA grants NAS1-99104 and NNX07AT11G and on the MODIS Science Team under NASA grant NNX08AG01G.

References

Albrecht, B. A. (1989), Aerosols, cloud microphysics and fractional cloudiness, *Science*, *245*, 1227–1230, doi:10.1126/science.245.4923.1227.

Boers, R., J. R. Acarreta, and J. L. Gras (2006), Satellite monitoring of the first indirect aerosol effect: Retrieval of the droplet concentration of water clouds, *J. Geophys. Res.*, *111*, D22208, doi:10.1029/2005JD006838.

Bony, S., and J.-L. Dufresne (2005), Marine boundary layer clouds at the heart of cloud feedback uncertainties in climate models, *Geophys. Res. Lett.*, *32*, L20806, doi:10.1029/2005GL023851.

Brenguier, J. L., H. Pawlowska, L. Schüller, R. Preusker, J. Fischer, and Y. Fouquart (2000), Radiative properties of boundary layer clouds: Droplet effective radius versus number concentration, *J. Atmos. Sci.*, *57*, 803–821, doi:10.1175/1520-0469(2000)057<0803:RPOBLC>2.0.CO;2.

Cahalan, R. F., W. Ridgway, W. J. Wiscombe, T. L. Bell, and J. B. Snider (1994), The albedo of fractal stratocumulus clouds, *J. Atmos. Sci.*, *51*, 2434–2455, doi:10.1175/1520-0469(1994)051<2434:TAOFSC>2.0.CO;2.

Chang, F.-L., and Z. Li (2003), Retrieving vertical profiles of water-cloud droplet effective radius: Algorithm modification and preliminary application, *J. Geophys. Res.*, *108*(D24), 4763, doi:10.1029/2003JD003906.

Chen, R., R. Wood, Z. Li, R. Ferraro, and F.-L. Chang (2008), Studying the vertical variation of cloud droplet effective radius using ship and spaceborne remote sensing data, *J. Geophys. Res.*, *113*, D00A02, doi:10.1029/2007JD009596.

Coakley, J. A., Jr., M. A. Friedman, and W. R. Tahnk (2005), Retrievals of cloud properties for partly cloudy imager pixels, *J. Atmos. Oceanic Technol.*, *22*, 3–17, doi:10.1175/JTECH-1681.1.

Eitzen, Z. A., K.-M. Xu, and T. Wong (2008), Statistical analyses of satellite cloud object data from CERES. part V: Relationships between physical properties of marine boundary layer clouds, *J. Clim.*, *21*, 6668–6688, doi:10.1175/2008JCLI2307.1.

Han, Q., W. B. Rossow, and A. A. Lacis (1994), Near-global survey of effective droplet radii in liquid water clouds using ISCCP data, *J. Clim.*, *7*, 465–497, doi:10.1175/1520-0442(1994)007<0465:NGSOED>2.0.CO;2.

Harshvardhan, G. Guo, R. N. Green, Z. Qu, and T. Y. Nakajima (2004), Remotely sensed microphysical and thermodynamic properties of nonuniform water cloud fields, *J. Atmos. Sci.*, *61*, 2574–2587, doi:10.1175/JAS3301.1.

Hartmann, D. L., M. E. Ockert-Bell, and M. L. Michelsen (1992), The effect of cloud type on Earth's energy balance: Global analysis, *J. Clim.*, *5*, 1281–1304, doi:10.1175/1520-0442(1992)005<1281:TEOCTO>2.0.CO;2.

Holz, R. E., S. A. Ackerman, F. W. Nagle, R. Frey, S. Dutcher, R. E. Kuehn, M. A. Vaughan, and B. Baum (2008), Global Moderate Resolution Imaging Spectroradiometer (MODIS) cloud detection and height evaluation using CALIOP, *J. Geophys. Res.*, *113*, D00A19, doi:10.1029/2008JD009837.

Kato, S., L. M. Hinkelman, and A. Cheng (2006), Estimate of satellite-derived cloud optical thickness and effective radius errors and their effect on computed domain-averaged irradiances, *J. Geophys. Res.*, *111*, D17201, doi:10.1029/2005JD006668.

Klein, S. A., and D. L. Hartmann (1993), The seasonal cycle of low stratiform clouds, *J. Clim.*, *6*, 1587–1606, doi:10.1175/1520-0442(1993)006<1587:TSCOLS>2.0.CO;2.

Loeb, N. G., and J. A. Coakley Jr. (1998), Inference of marine stratus cloud optical depths from satellite measurements: Does 1-D theory apply?, *J. Clim.*, *11*, 215–233, doi:10.1175/1520-0442(1998)011<0215:IOMSCO>2.0.CO;2.

Mahesh, A., M. A. Gray, S. P. Palm, W. D. Hart, and J. D. Spinhirne (2004), Passive and active detection of clouds: Comparisons between MODIS and GLAS observations, *Geophys. Res. Lett.*, *31*, L04108, doi:10.1029/2003GL018859.

Matheson, M. A., J. A. Coakley Jr., and W. R. Tahnk (2005), Aerosol and cloud property relationships for summertime stratiform clouds in the northeastern Atlantic from Advanced Very High Resolution Radiometer observations, *J. Geophys. Res.*, *110*, D24204, doi:10.1029/2005JD006165.

Matheson, M. A., J. A. Coakley Jr., and W. R. Tahnk (2006), Effects of threshold retrievals on estimates of the aerosol indirect radiative forcing, *Geophys. Res. Lett.*, *33*, L07705, doi:10.1029/2005GL025614.

Miles, N. L., J. Verlinde, and E. E. Clothiaux (2000), Cloud droplet size distributions in low-level stratiform clouds, *J. Atmos. Sci.*, *57*, 295–311, doi:10.1175/1520-0469(2000)057<0295:CDSDIL>2.0.CO;2.

Platnick, S., and L. Oreopoulos (2008), Radiative susceptibility of cloudy atmospheres to droplet number perturbations: 1. Theoretical analysis

and examples from MODIS, *J. Geophys. Res.*, *113*, D14S20, doi:10.1029/2007JD009654.

Platnick, S., M. D. King, S. A. Ackerman, W. P. Menzel, B. A. Baum, J. C. Riedi, and R. A. Frey (2003), The MODIS cloud products: Algorithms and examples from Terra, *IEEE Trans. Geosci. Remote Sens.*, *41*, 459-473, doi:10.1109/TGRS.2002.808301.

Randall, D., M. Khairoutdinov, A. Arakawa, and W. Grabowski (2003), Breaking the cloud parameterization deadlock, *Bull. Am. Meteorol. Soc.*, *84*, 1547–1564, doi:10.1175/BAMS-84-11-1547.

Schüller, L., R. Bennartz, J. Fischer, and J.-L. Brenguier (2005), An algorithm for the retrieval of droplet number concentration and geometrical thickness of stratiform marine boundary layer clouds applied to MODIS radiometric observations, *J. Appl. Meteorol.*, *44*, 28–38, doi:10.1175/JAM-2185.1.

Segrin, M. S., J. A. Coakley Jr., and W. R. Tahnk (2007), Summertime observations of ship tracks off the west coast of the U.S. in MODIS Terra and Aqua data, *J. Atmos. Sci.*, *64*, 4330–4345, doi:10.1175/2007JAS2308.1.

Stevens, B., G. Vali, K. Comstock, R. Wood, M. C. van Zanten, P. H. Austin, C. S. Bretherton, and D. H. Lenschow (2005), Pockets of open cells and drizzle in marine stratocumulus, *Bull. Am. Meteorol. Soc.*, *86*, 51–57, doi:10.1175/BAMS-86-1-51.

Szczodrak, M., P. H. Austin, and P. B. Krummel (2001), Variability of optical depth and effective radius in marine stratocumulus clouds, *J. Atmos. Sci.*, *58*, 2912–2926, doi:10.1175/1520-0469(2001)058<2912:VOODAE>2.0.CO;2.

Vaughan, M., K. Powell, R. Kuehn, S. Young, D. Winker, C. Hostetler, W. Hunt, Z. Liu, M. McGill, B. Getzewich (2010), Fully automated detection of cloud and aerosol layers in the CALIPSO lidar measurements, *J. Atmos. Oceanic Technol.*, *26*(10), 2034–2050, doi:10.1175/2009JTECHA1228.1.

Winker, D. M., M. A. Vaughan, A. H. Omar, Y. Hu, K. A. Powell, Z. Liu, W. H. Hunt, and S. A. Young (2010), Overview of the CALIPSO mission and CALIOP data processing algorithms, *26*(11), 2310–2323, *J. Atmos. Oceanic Technol.*, doi:10.1175/2009JTECHA1281.1.

Wood, R., and C. S. Bretherton (2006), On the relationship between stratiform low cloud cover and lower-tropospheric stability, *J. Clim.*, *19*, 6425–6432, doi:10.1175/JCLI3988.1.

J. A. Coakley Jr., C. R. Hayes, and W. R. Tahnk, College of Oceanic and Atmospheric Sciences, Oregon State University, 104 COAS Administration Bldg., Corvallis, OR 97331-5503, USA. (coakley@coas.oregonstate.edu)